Electronic Supplementary Material (ESI) for Materials Horizons.
This journal is © The Royal Society of Chemistry 2022

Supporting Information

Quantitative High-Throughput Measurement of Bulk Mechanical Properties Using Commonly Available Equipment

Justin Griffith*[1], Yusu Chen*[1], Qingsong Liu[1], Qifeng Wang[2], Jeffrey Richards[1], Danielle Tullman-Ercek[1], Kenneth Shull[2], Muzhou Wang[1]

*These authors contributed equally to this work.

[1]Department of Chemical and Biological Engineering, [2]Department of Materials Science & Engineering, Northwestern University, Evanston, IL 60208, United States

Table S1: Average shear modulus (kPa) for PAM and triblock gels across all used concentrations. Storage (G') and loss moduli (G") were recorded over a frequency range of 0.1-100 rad/s at 5% strain (Figure S9), and shear modulus was taken to be equivalent to storage modulus at a frequency of 1 rad/s.

Concentration (wt%)	PAM Shear Modulus (kPa)	Triblock Shear Modulus (kPa)
4	0.771	0.117
6	3.149	0.425
8	7.278	0.994
10	13.02	1.465
12	19.94	1.856
14	31.19	2.346
16	37.62	3.140
18	46.65	3.369
20	56.07	3.889

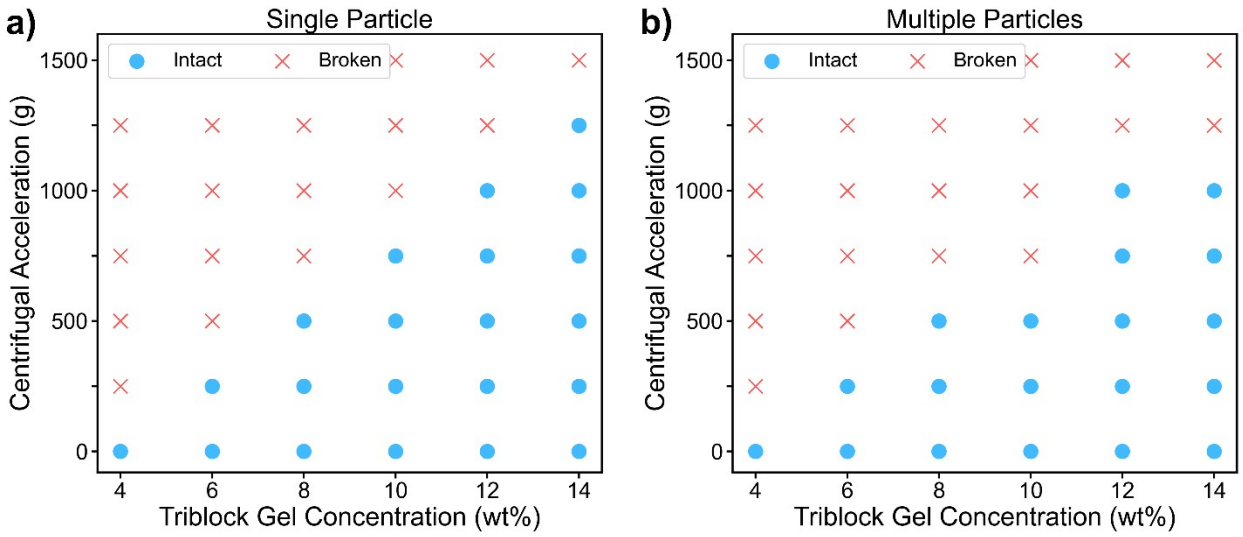

Figure S1: Centrifugal results from (a) a single particle in the middle of each well and (b) multiple particles in each well. Centrifugation was performed in a 96-well plate with 1 mm diameter stainless steel particles. A U-shaped well plate was used for the single particle test to keep the particle in the middle of the well, and a flat-bottomed plate was used for the multiple particles test. 100 µL of triblock gel was added to each well in both cases. Centrifugal acceleration at fracture was consistent within error for both scenarios.

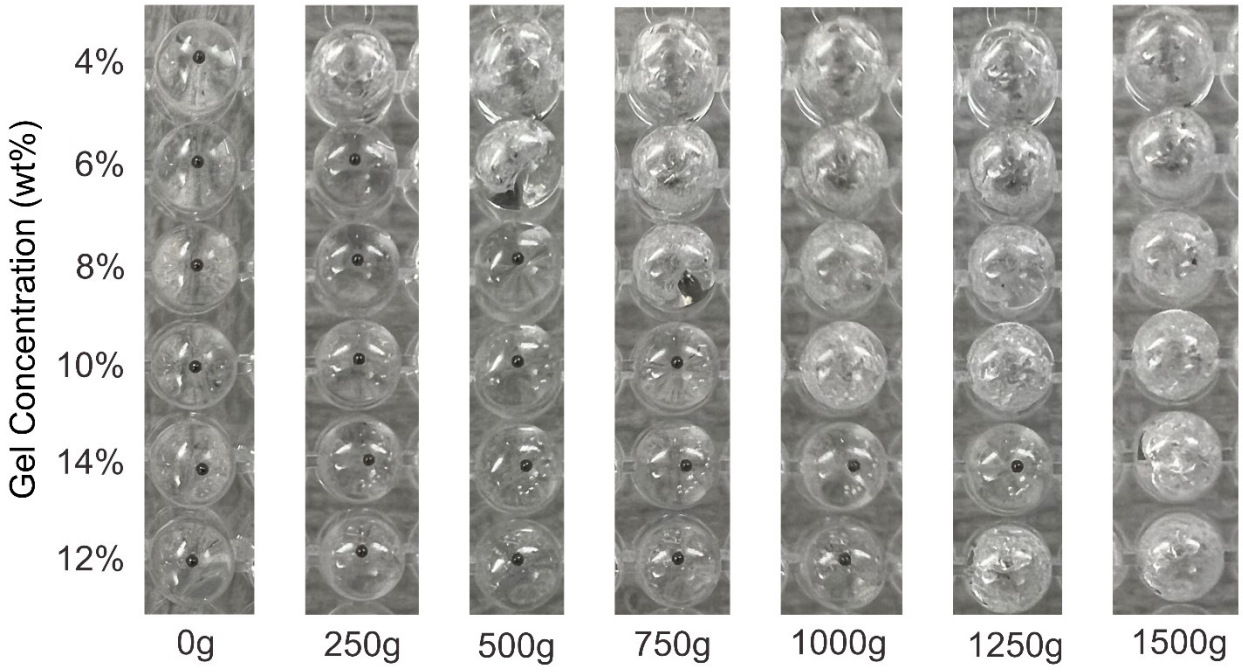

Figure S2: Photographs of single particle centrifugal experiment as described in figure S1. The same row in the well plate is shown from the bottom after cycles at increasing speeds. When a sample fractures, the particle breaks through to the top of the well plate and are thus not visible in subsequent photos.

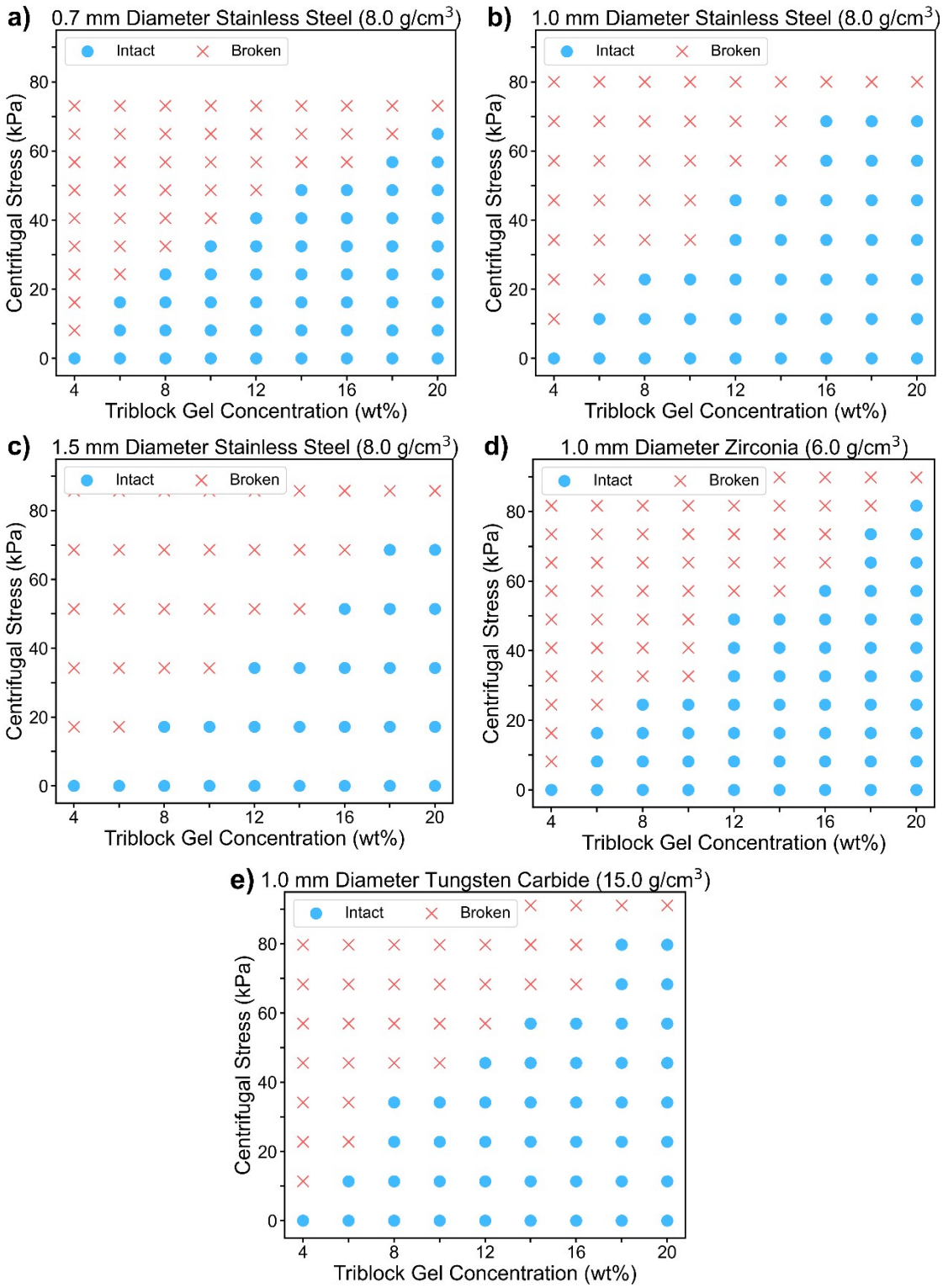

Figure S3: Centrifugal results for triblock gels in a 96-well plate using (a) 0.7 mm diameter stainless steel particles, (b) 1 mm diameter stainless steel particles, (c) 1.5 mm diameter stainless steel particles, (d) 1 mm diameter yttria-stabilized zirconia particles, and (e) 1 mm diameter tungsten carbide particles. Stainless steel particles had a density of 8.0 g/cm^3, zirconia particles had a density of 6.0 g/cm^3, and tungsten carbide particles had a density of 14.95 g/cm^3. 100 µL of gel solution was added to each well in all tests. Results were consistent for all particle types.

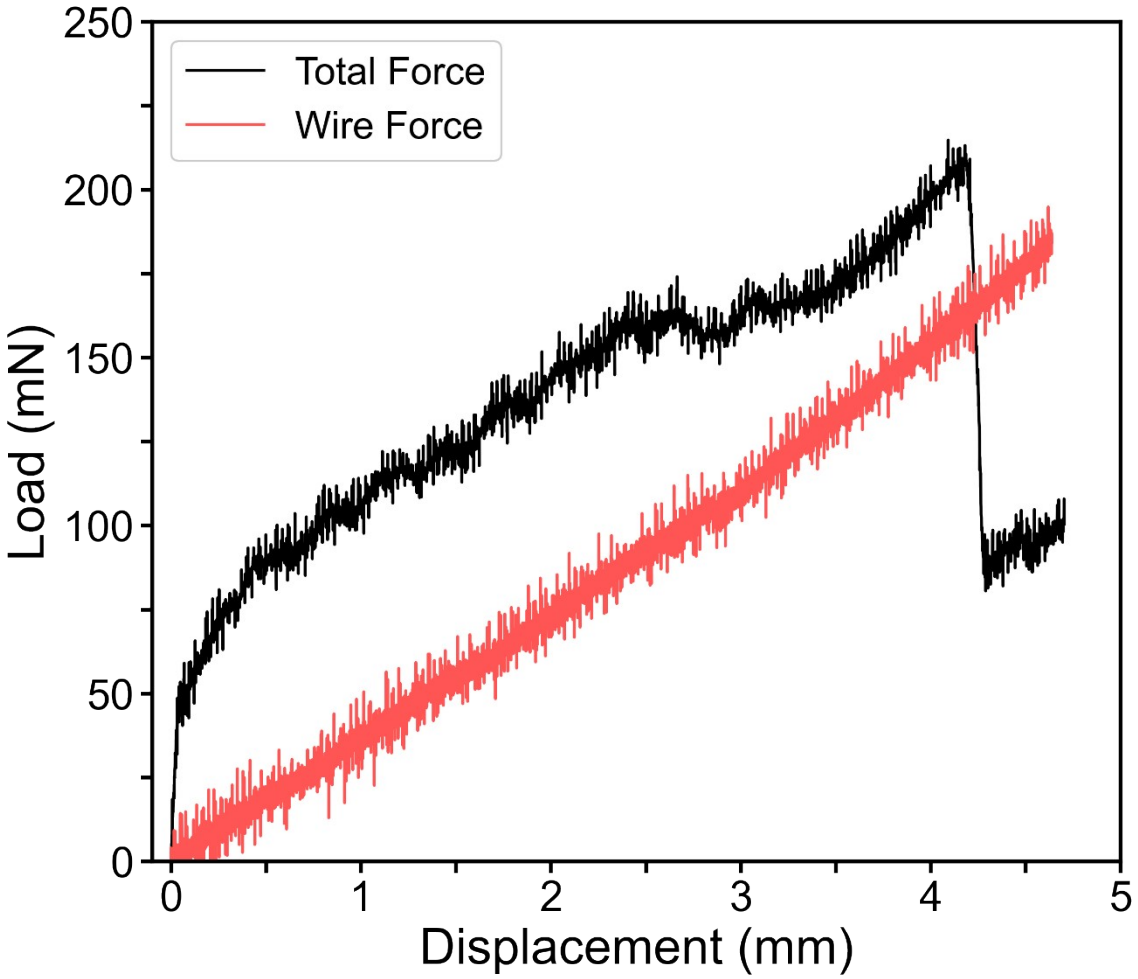

Figure S4: Force vs displacement in particle pulling experiment. Total force includes forces both on the particle and on the wire. For total force, a 3 mm diameter stainless steel particle attached to a 0.01-inch diameter metal wire was started at the bottom of a 15 mm tall 10 wt% triblock gel and was pulled upwards at 20 μm/s using a piezoelectric stepping motor. Force and displacement were recorded using a load transducer and optical sensor until just after the gel fractured. For wire-only control experiment, the same wire was started 3 mm above the bottom of the gel without a particle attached and pulled upwards under identical conditions.

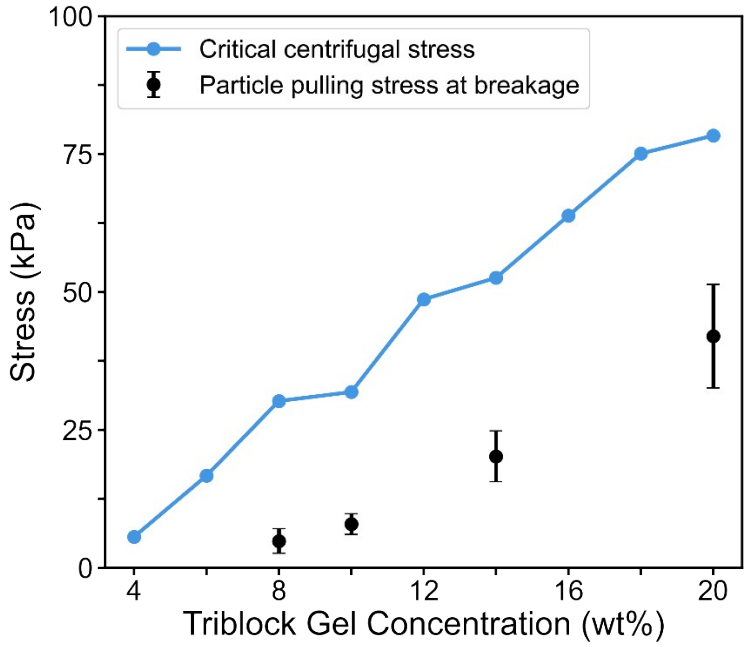

Figure S5: Critical centrifugal stress correlated to stress on the particle at fracture in the particle pulling experiment (mean ± s.d.). Particle pulling was carried out as described in Figure S4. Particle pulling stress was calculated by subtracting the force of the wire from the total force at fracture and normalizing the result by the particle area. Centrifugation was carried out in a 96-well plate and critical centrifugal stress was averaged across all types of particles seen in Figure S3. 100 µL of triblock gel was added to each well in all centrifugal tests.

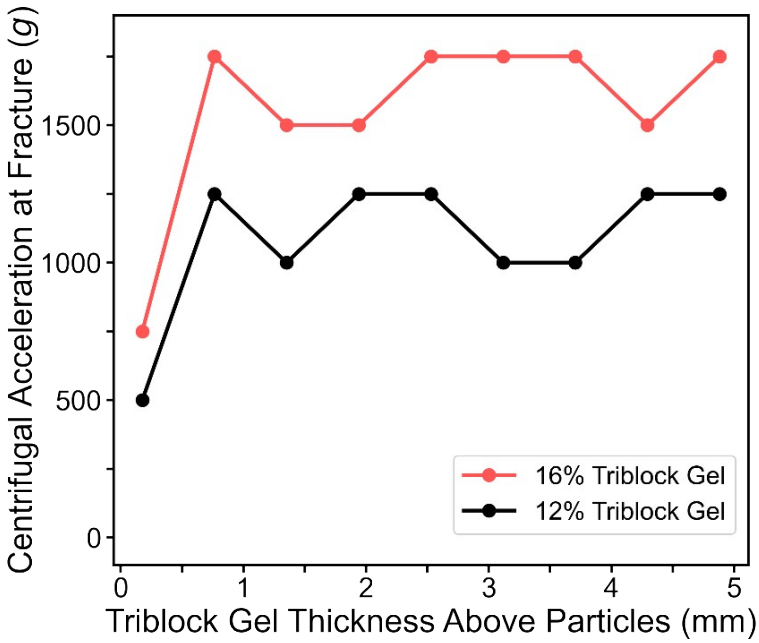

Figure S6: Effect of varying thickness of gel above particles for 12 wt% and 16 wt% triblock gels. Centrifugation was performed in a 96-well plate with 1 mm diameter stainless steel particles. For both systems, the centrifugal acceleration at fracture was constant within error above 2 mm gel thickness.

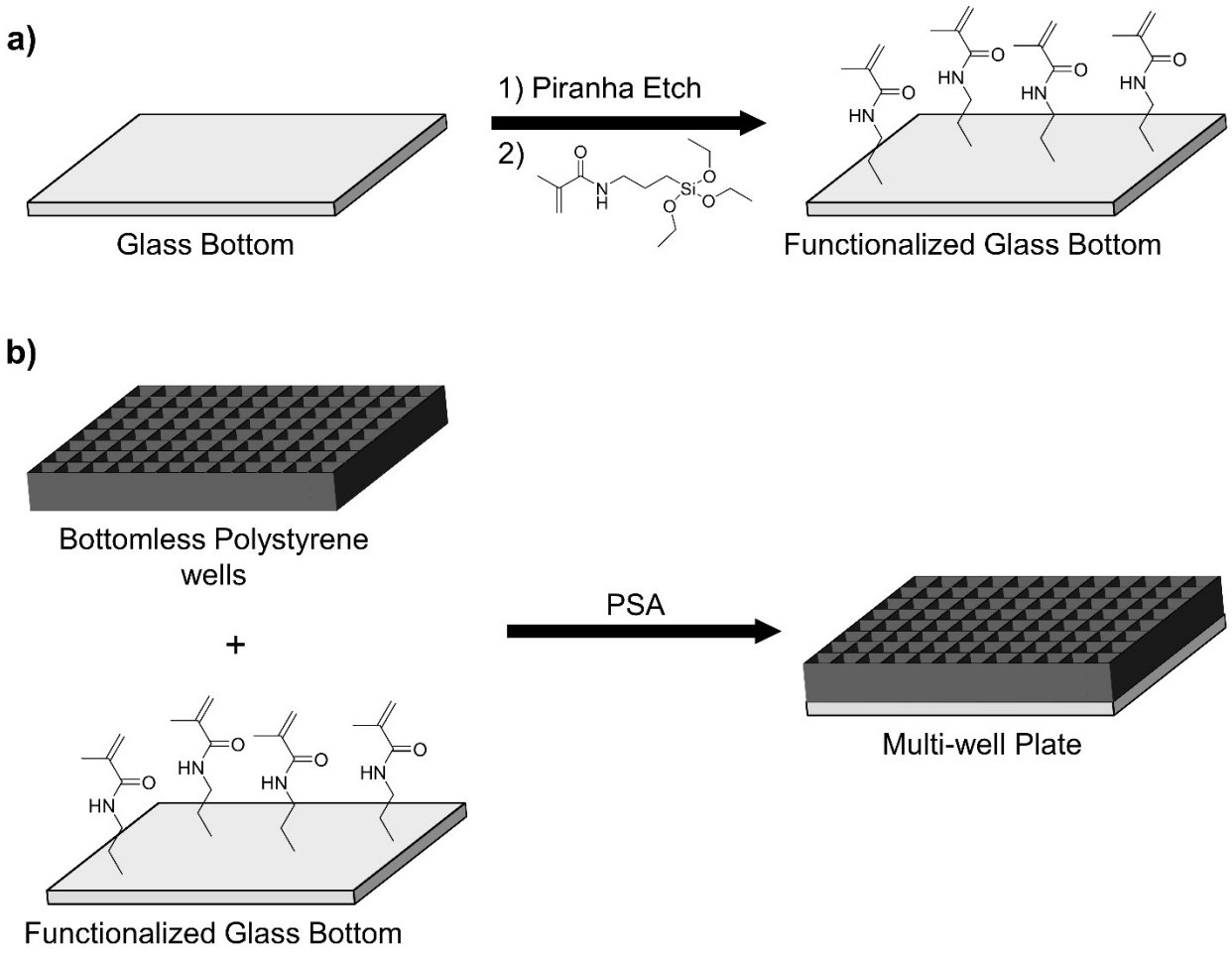

Figure S7: Diagram of separable glass-bottom well plate used for functionalization. (a) Glass bottom is etched with piranha solution and subsequently reacted with a silane coupling agent to deposit methacrylamide groups on the glass. (b) Bottomless polystyrene wells are attached to functionalized glass bottom using a pressure-sensitive adhesive on the bottom of the wells, forming a tight seal.

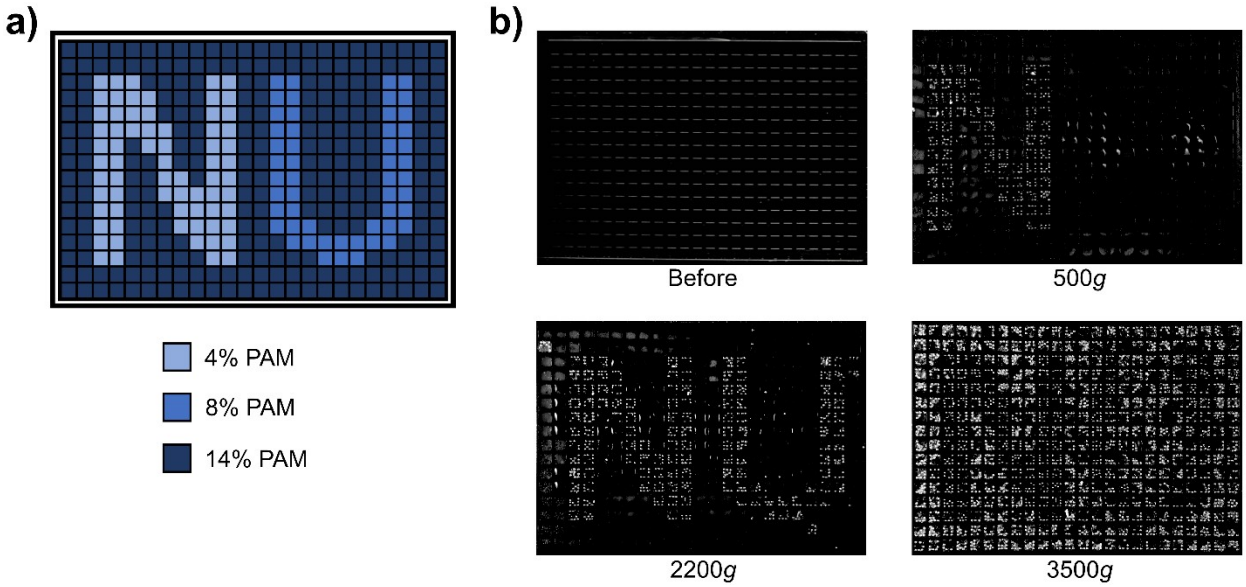

Figure S8: Full 384-well plate centrifugation experiment using 1 mm diameter stainless steel particles. (a) Pre-determined pattern of material samples. 40 μL of polyacrylamide solution at the specified concentration was added to each well. (b) Photographs of experimental results of full plate experiment. The plate is shown from the top after centrifugation cycles at different speeds, so particles are only visible once they break out of the gel. Particles start at the bottom of the wells, so none are visible prior to centrifugation, and more particles in the pattern become visible at higher speeds. Photos shown are unprocessed.

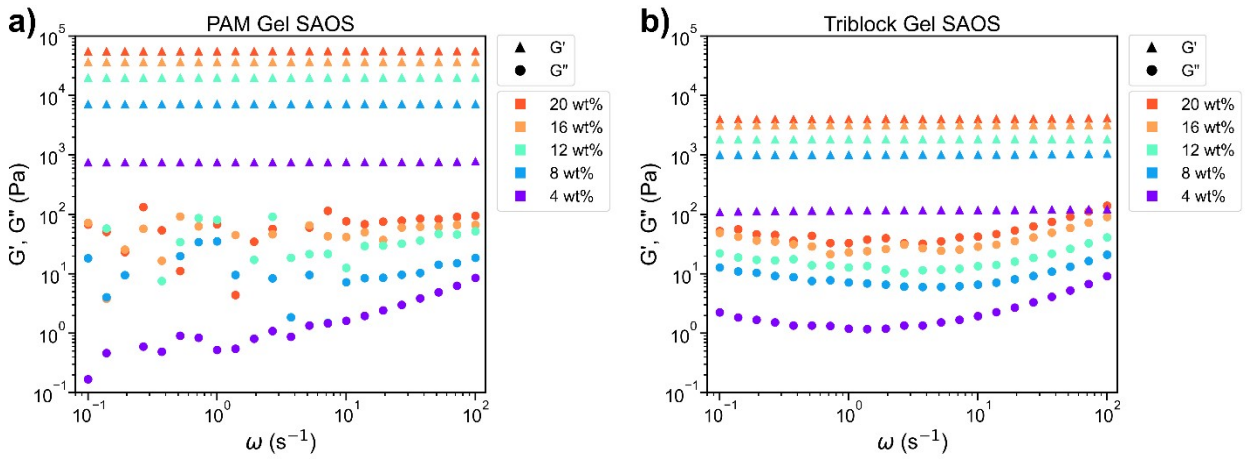

Figure S9: Storage modulus (G', triangular markers) and loss modulus (G", circular markers) obtained from small-amplitude oscillatory shear experiments conducted on (a) PAM gels and (b) triblock gels of different compositions. All experiments were conducted at 5% strain.

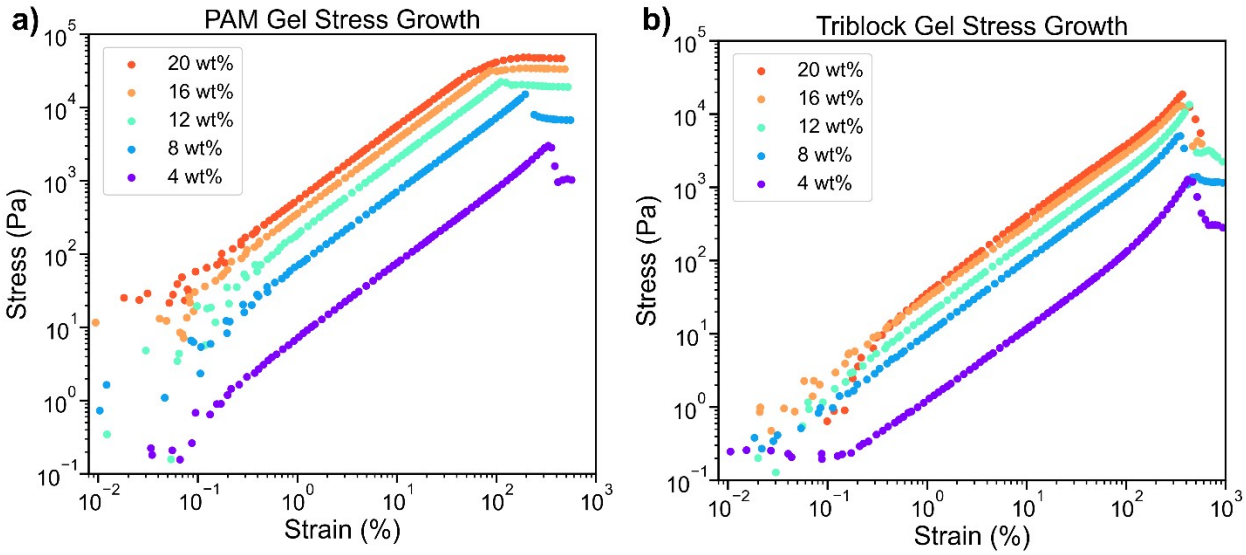

Figure S10: Stress growth experiments conducted on (a) PAM gels and (b) triblock gels of different compositions. Strain was increased at a rate of 0.05 s^{-1}. Fracture stress was recorded as the highest stress reached during the experiment.

Deformation field around a sphere under a linear force in an infinite solid medium

A linear momentum balance provides a set of equations for the Cauchy stress tensor field,

$$\frac{\partial \sigma_{ij}}{\partial x_i} = 0\,, \tag{S1}$$

where x is the Cartesian position coordinate, and we use index notation for convenience. We assume linear elasticity in an isotropic medium at constant temperature to give the constitutive relation,

$$\sigma_{ij} = \frac{E}{1+\nu}\left(\varepsilon_{ij} + \frac{\nu}{1-2\nu}\varepsilon_{kk}\delta_{ij}\right), \tag{S2}$$

where E is Young's modulus, ν is Poisson's ratio, $\boldsymbol{\delta}$ is the identity tensor, and $\boldsymbol{\varepsilon}$ is the infinitesimal strain tensor field given by,

$$\varepsilon_{ij} = \frac{1}{2}\left(\frac{\partial u_i}{\partial x_j} + \frac{\partial u_j}{\partial x_i}\right), \tag{S3}$$

where $\mathbf{u}$ is the deformation vector field. A more convenient formulation of this constitutive relation is in terms of the bulk modulus $K = E/3(1\text{-}2\nu)$ and the shear modulus $G = E/2(1+\nu)$,

$$\sigma_{ij} = K\varepsilon_{kk}\delta_{ij} + 2G\left(\varepsilon_{ij} - \tfrac{1}{3}\varepsilon_{kk}\delta_{ij}\right). \tag{S4}$$

This expression is helpful because the second term is traceless, so the first term is related to a scalar pressure, and the second is related to shear forces. Here we assume the medium is incompressible ($\nu = 0.5$), which is an excellent approximation for the two systems studied in this work, as well as most other polymers and soft materials. In this case, the trace of the strain tensor is identically zero,

$$\varepsilon_{kk} = \frac{\partial u_k}{\partial x_k} = 0\,. \tag{S5}$$

However, the bulk modulus becomes infinite for an incompressible material, so the first term of Equation S4 is indeterminate, and is conventionally replaced by a hydrostatic pressure P. The constitutive relation thus reduces to the more familiar expression,

$$\sigma_{ij} = -P\delta_{ij} + 2G\varepsilon_{ij}\,. \tag{S6}$$

We substitute this relation into the linear momentum balance (Equation S1) using the definition of $\boldsymbol{\varepsilon}$ (Equation S3) to find,

$$-\frac{\partial P}{\partial x_j} + G\left(\frac{\partial^2 u_j}{\partial x_i \partial x_i} + \frac{\partial}{\partial x_j}\left(\frac{\partial u_i}{\partial x_i}\right)\right) = 0\,. \tag{S7}$$

The last term of the left-hand side vanishes due to incompressibility (Equation S5). The result becomes,

$$\begin{aligned} -\frac{\partial P}{\partial x_j} + G\frac{\partial^2 u_j}{\partial x_i \partial x_i} &= 0 \\ -\nabla P + G\nabla^2 \mathbf{u} &= 0 \end{aligned}\,. \tag{S8}$$

One may notice that this analysis exactly follows the derivation of the familiar Navier-Stokes equations from fluid mechanics. In fact, our result is identical to the Stokes equation for steady low Reynolds number flows, but our equation is for the deformation field **u** rather than the velocity field **v**, and we use the shear modulus G rather than the viscosity μ. This is a demonstration of the correspondence principle of viscoelasticity.[1,2]

Our desired situation is to solve for the deformation field when a sphere moves a distance of U relative to an infinite solid medium. The corresponds exactly to the situation of a sphere moving with a velocity of U in an infinite fluid medium. As this is a very familiar problem taught in most fluid mechanics courses, and the derivation can be found in many sources,[3] we do not repeat it here. The result is provided in Equation 2 of the main body.

References

[1] A. C. Pipkin, *Lectures on Viscoelastic Theory*, Springer-Verlag, New York, **1986**.

[2] E. M. Furst, T. M. Squires, *Microrheology*, Oxford University Press, **2017**.

[3] W. M. Deen, *Analysis of Transport Phenomena*, Oxford University Press, **2011**.